Engineering Structures 127 (2016) 227–239

Contents lists available at ScienceDirect

Engineering Structures

journal homepage: www.elsevier.com/locate/engstruct

Impact of the reinforcement layout on the load capacity of reinforced concrete half-joints

Pieter Desnerck *, Janet M. Lees, Chris T. Morley

University of Cambridge, Department of Engineering, Concrete and Composites Structures Group, Trumpington Street, CB2 1PZ Cambridge, United Kingdom

ARTICLE INFO

Article history:
Received 4 May 2016
Revised 5 August 2016
Accepted 30 August 2016
Available online 13 September 2016

Keywords:
Assessment
Dapped-end beam
Half-joint
Strut-and-tie
Load-bearing capacity
Reinforcement detailing
Re-entrant corner

ABSTRACT

A reinforced concrete half-joint beam has a complex geometry that includes both a locally disturbed nib region and a full depth section. While this configuration simplifies the design and construction procedures, half joint structures rely on the internal steel reinforcement to transfer force from the nib into the bulk of the beam. When assessing existing reinforced concrete half-joints, engineers can be confronted with internal reinforcement layouts that do not correspond to the as-designed drawings and/or do not comply with current design practice. Bars may be missing or the location, percentage and spacing of the steel reinforcing bars may be non-compliant.

To provide a better understanding of the contribution of the internal steel reinforcing bars found in a typical half joint detail, an experimental test program on full-scale half-joint beams was undertaken. Four different scenarios were tested to identify the impact of specific reinforcing bars. A reference specimen was designed in accordance with existing practice. The reference beam, and beams with either missing diagonal reinforcement, missing horizontal reinforcement or a reduced amount of shear reinforcement were tested.

All the beams exhibited nib failures with the exception of the beam where the shear reinforcement was reduced. In this case, the failure mode changed from a nib failure to a full-depth failure. The results indicated that if certain bars are missing the overall load bearing capacity of a half-joint could be approximately 40% lower than that of a properly designed detail, but that a redistribution of forces was noted.

1. Introduction

A reinforced concrete half joint bridge is characterised by a suspended span supported on the nibs of abutments or adjacent beams (Fig. 1). Within the existing UK Highways England network alone there are over 400 concrete bridges with half joints [1,2]. Advantages of this structural form are the suitability for pre-cast construction [3] and a reduced construction depth with a level running surface along the bridge deck and the support spans.

In a half-joint, the reinforcement detailing to ensure the transfer of forces from the load point, through the nib, and into the full depth section is critical. Half joint details have come under scrutiny since the collapse of a section of the de la Concorde Overpass in Quebec, Canada in 2006 [4]. Five people were killed and six others injured [5]. Thus, a key challenge is to understand the inherent vulnerabilities in half joint structures.

Half-joint beams, also referred to as dapped end beams, typically follow one of two main reinforcement design layouts. One approach, often used in Europe, is to provide diagonal reinforcement to transfer (part of) the applied load from the nib to the full-depth section of the beam (Fig. 2a). A second approach (Fig. 2b), more common in the US, is to provide a substantial amount of longitudinal reinforcement in the nib that extends sufficiently far into the full-depth section and intersects with vertical transverse hanger reinforcing steel. In order for this longitudinal reinforcement to be properly anchored in the nib itself, anchorage plates are welded to the reinforcement. For half-joints with diagonal reinforcing bars, strut-and-tie methods (STM) provide a basis for the design of the steel in the D-region around the nib [6]. For layouts such as that shown in Fig. 2b, strut-and-tie methods [7] or simplified design equations such as those given in the PCI Design handbook [8] can be used.

The influence of the internal reinforcement detail on the performance of a half-joint has been investigated experimentally. In 1975, Hamoudi et al. [9] performed tests on eight half joint beams, some specimens with, and some without, diagonal bars. They identified two potential failure modes for reinforced concrete half-joints: a nib failure with a crack extending from the inner nib at an angle inclined to the longitudinal axis of the beam and a flexural

* Corresponding author.
E-mail address: Pieter.Desnerck@eng.cam.ac.uk (P. Desnerck).

http://dx.doi.org/10.1016/j.engstruct.2016.08.061
0141-0296/

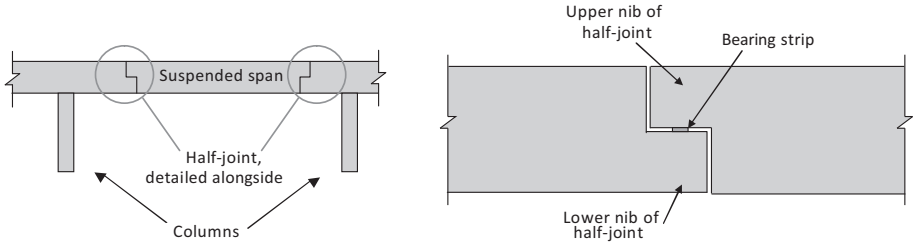

Fig. 1. Half-joint principle for reinforced concrete bridges.

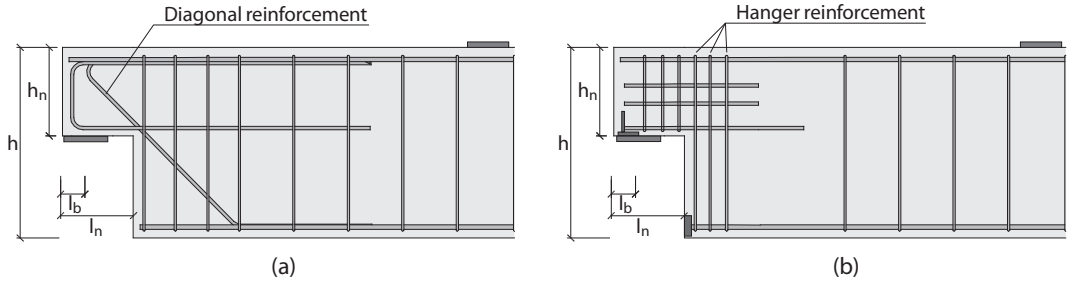

Fig. 2. Different reinforcement layout approaches for the design of half-joints.

failure in the full depth section. Mattock and Chan [3] confirmed these failure modes by performing tests on four half joint beams but identified a third failure plane originating from the bottom corner of the full-depth section. The specimens were designed according to corbel design principles at the time (no diagonal bars were provided) and the location and amount of hanger reinforcement varied. The test results emphasised the importance of proper anchorage of the longitudinal reinforcing bars in the nib and the need to provide sufficient hanger reinforcement. Tests performed by Mitchell et al. [10] led to the same conclusion. Specimens with properly detailed reinforcement developed up to a 30% greater strength than beams with improper detailing. Closed stirrups provided better end anchorage and are to be preferred over U-stirrups. For wider beams, closed stirrups with multiple legs were shown to be the most effective.

Steinle and Rostasy [11] and Clark and Thorogood [12] performed tests on half-joints with and without diagonal reinforcing bars. Both concluded that the diagonal reinforcement highly influences the service load behaviour of the half-joint. Clark and Thorogood reported that the maximum crack widths at the re-entrant can be six times higher in the absence of these diagonal reinforcing bars. In addition, they showed that the crack pattern was influenced by the type of bearing. Soft rubber bearings lead to increased crack widths and a more extensive crack pattern. Therefore, they advise using hard bearings instead of soft rubber bearings.

More recent studies [13,14] on 1000 mm wide half-joint specimens confirmed the importance of diagonal reinforcement in controlling the crack width at the re-entrant corner. When only vertical hanger reinforcement was provided, the specimens cracked at a lower load and the initial crack widths were higher. The specimen with diagonal bars also showed a higher stiffness. However, the maximum crack width of all tested specimens remained below 0.1 mm. An important factor in the control of cracking, in addition to the presence of the diagonal reinforcement, is the proximity of the first stirrup to the nib [15]. Wang et al. recommended that the first stirrup should be placed as close as possible to the edge of the nib (taking into account cover requirements) and that $0.45 \cdot h$ (where h is the height of the full depth section) should be used as a minimal nib height to avoid local shear failures.

The shear strengths of half joints have been found to increase with decreasing span-to-depth ratios a/d (with d the effective height of the full depth section) and increasing concrete compressive strength [16]. Both the ultimate failure load and the stiffness increased with decreasing a/d. On the other hand, horizontal forces acting on the nib had a negative impact on the load capacity. As most half-joint failure modes are brittle in nature, Lu et al. [17] recommended the use of higher strength concretes and low flexural tensile reinforcement ratios to ensure sufficient ductility.

So far only limited research has been done on the calibration of finite element models for half-joint applications. The analysis conducted by Boothman et al. [18] showed satisfactory results, but the authors emphasize the applicability is limited to half-joints with highly similar geometry and load conditions. Debonding mechanisms were not modelled, and hence assessments, using their FE model, of cases with poor detailing or with severe cracking in anchorage zones should be conducted with great care.

Design guidelines such as the PCI Design handbook have been updated on a regular basis to implement the findings of the reported studies. However, more recent work by Mitchell et al. [10] showed that some of the recommendations might still lead to the improper anchorage of the longitudinal reinforcement at the top and bottom of a beam and this has been identified by Taher [19] as the most critical reinforcement detail. In addition, Yang et al. [20] claim that the influence of the amount of hanger, longitudinal and shear reinforcing bars in the nib is still not reasonably represented in the PCI design method.

A further challenge with existing infrastructure is when inspections [21] reveal reinforcement layouts that do not correspond to the as-designed requirements [22] or details that do not comply with standard strut-and-tie approaches. Specific guidelines [1,2,23] have been developed for the assessment of existing reinforced concrete half-joints, but these documents mainly relate to the effects of corrosion and crack widths. With respect to the expected ultimate load capacity little or no guidance is provided except to state that appropriate strut-and-tie models should be used. Assessment decisions for non-compliant cases are therefore often at the discretion of Engineers who potentially have limited experimental evidence for the possible redistribution of forces or unforeseen failure modes. Furthermore, current standards such

as the PCI guidelines can lead to conservative estimates of the load carrying capacity [24] when the provided reinforcement does not comply with minimum reinforcement requirements.

To help fill this knowledge gap, an experimental study has been undertaken to study the effect of changes in the reinforcement layout on the behaviour of reinforced concrete half-joints. The study aims to provide the experimental basis for the determination of the load capacity of reinforced concrete half-joints that do not comply with currently accepted design principles and hence lead to uncertainty when being assessed. A particular focus was the impact of the absence of specific sets of reinforcing bars.

2. Experimental design

To investigate the influence of the reinforcement layout on the load-bearing capacity of reinforced half-joints, four different scenarios were tested.

2.1. Specimen geometry

Common design ratios for reinforced concrete half-joints were extracted from the literature. The selected references consisted of laboratory studies on relatively small specimens as well as reports with design drawings of existing reinforced concrete half-joint structures. Table 1 summarizes the dimensions, scale (full scale or lab scale) as well as the chosen reinforcement design layout (see Fig. 2). On average, the height of the nib h_n (the notation is shown in Fig. 2) was 51% of the overall full height h with the majority of the full-scale structures having a ratio of around 0.45 (which is in line with the minimum value specified by Wang et al. [15]). This is a consequence of the symmetrical design that takes into account the thickness of the bearing pad in between the supporting half-joint and half-joint drop-in span. The length of the nib l_n is often shorter than the height, with an average ratio of 90%. The location of the centre of the loading point l_b does not typically coincide with the middle of the nib but is instead slightly shifted towards the outer edge (due to the provision of an expansion joint in real bridge applications).

The obtained ratios were used to design the half-joints considered in this experimental program. As the aim was to test full-scale beams to thereby limit size effects, the height of the specimen was chosen to be 700 mm. Based on the obtained average ratios of h_n/h, l_n/h_n and l_b/l_n (Table 1), the overall dimensions of the specimen were then determined (see Fig. 3). The specimens were designed as beams with two different half-joint ends, resulting in two test scenarios for each beam.

The nib of a half joint beam can be considered as a structural concrete region with statical or geometrical discontinuities and hence is a D-region (disturbed or discontinuity), while the other regions of the beam are referred to as B-regions (Bernoulli or

Table 1
Common dimensions and dimensional ratios of reinforced concrete half-joints as reported in literature.

Ratio	h [mm]	h_n [mm]	l_b [mm]	l_n [mm]	Reinf. layout [a]	Test scale [b]	h_n/h [–]	l_n/h_n [–]	l_b/l_n [–]
Hamoudi et al. [9]	813	355–558	107–203	215–406	A - B	LS	0.43–0.69	0.28–1.14	0.50
Mattock and Chan [3]	610	305	101.5	203	B	LS	0.50	0.67	0.50
Clark and Thorogood [12]	460	210	100–175	250	A	LS	0.46	1.19	0.40–0.70
Cook and Mitchell [25]	600	250	37.5	137.5	B	LS	0.42	0.55	0.27
Barton [26]	785	430	101.5	203	A	LS	0.55	0.47	0.50
	785	430	101.5	203	B	LS	0.55	0.47	0.50
Mitchell and Cook [7]	400	200	50	200	B	LS	0.50	1.00	0.25
Mader [27]	699	330	114	228	A - B	LS	0.47	0.69	0.50
Bergmeister et al. [28]	762	406	127	254	B	FS	0.53	0.63	0.50
ACI Committee 445-1 [29]	483	229	76	177	B	FS	0.47	0.77	0.43
Lu et al. [24]	600	300	150	300	B	LS	0.50	1.00	0.50
Wang et al. [15]	370	160–190	75	150	A - B	LS	0.43–0.51	0.79–0.94	0.50
	300	150	75	150	A - B	LS	0.50	1.00	0.50
Smith [30]	2300	1019	200	559	B	FS	0.44	0.55	0.36
	2000	854	250	725	B	FS	0.43	0.85	0.34
Martin and Sanders [31]	762	381	190.5	381	B	FS	0.50	1.00	0.50
Prestressed Concrete Institute [8]	711	406	63.5	152	B	FS	0.57	0.37	0.42
Boothman et al. [18]	900	450	250	600	A	FS	0.50	1.33	0.42
Mohamed and Elliott [32]	600	400	100	200	B	LS	0.67	0.50	0.50
Amie [33]	3300	1600	300	762	n/a	FS	0.48	0.48	0.39
	1143	546	248	508	n/a	FS	0.48	0.93	0.49
Mitchell et al. [10]	600	300	80	230	B	LS	0.50	0.77	0.35
Santhanam and Shah [22]	533	260	140	292	B	FS	0.49	1.12	0.48
Mitchell et al. [5]	1156	508	203	457	A	FS	0.44	0.90	0.44
Lu et al. [16]	600	300	220	300	B	LS	0.50	1.00	0.73
	600	300	330	600	B	LS	0.50	2.00	0.55
Moreno and Meli [13]	480	250	125	275	A - B	LS	0.52	1.10	0.45
Popescu et al. [34]	1500	800	125	800	B	LS	0.53	1.00	0.16
Ahmad and Elahi [35]	457	279	66	127	B	LS	0.61	0.46	0.52
	305	178	66	127	B	LS	0.58	0.71	0.52
Aswin et al. [36]	250	140	55	110	B	LS	0.56	0.79	0.50
Lu et al. [17]	600	300	50	500	B	LS	0.50	1.67	0.10
Taher [19]	300	150	100	300	B	LS	0.50	2.00	0.33
						Average	0.51	0.90	0.44
						St Dev	0.05	0.41	0.12

[a] A = reinforcement layout with diagonal reinforcement, B = increased longitudinal and shear reinforcement in nib (see Fig. 2).
[b] LS = Laboratory scale, FS = Full scale, n/a = information not available.

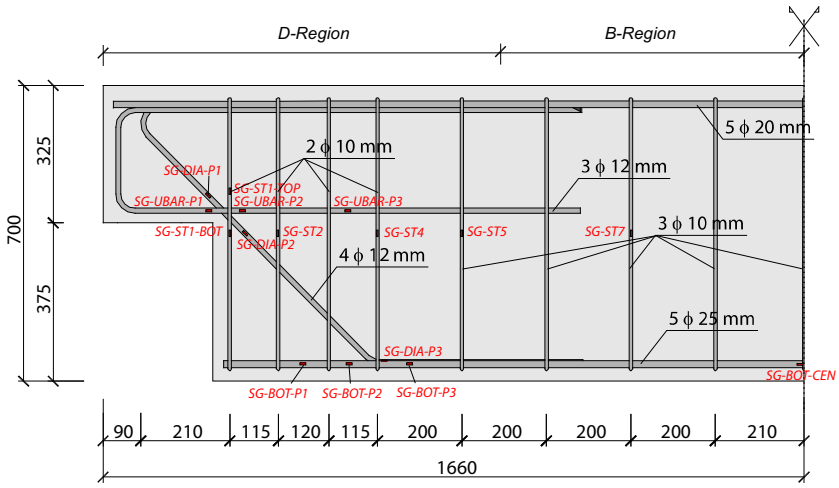

Fig. 3. Geometry and dimensions of experimental half-joint specimen.

beam). In B-regions, the design is based on bending and shear theory, and the Bernoulli assumption of 'plane sections remain plane' is valid. In D-regions, due to the discontinuities, this assumption is not valid and the design is based on alternative methods such as strut-and-tie approaches [6]. In general, it can be assumed that D-regions extend a distance h (with h defined as the full depth half-joint beam height) from the discontinuity itself [37]. Using a strut-and-tie approach and applying a design load of 300 kN, the reinforcement layout in the D-region (see Fig. 3) was designed assuming the concrete to have a compressive strength of 30 MPa and the yield stress of the reinforcement to be 500 MPa. No material safety factors were applied. The chosen approach included diagonal bars in the reference specimen, as this is a common detail in bridges in England. In the B-region of the beam, a flexural design and shear check was performed. Sufficient longitudinal and shear reinforcement were provided to avoid premature failure of the reference specimen by bending or shear in the B-region.

A total of 5 bars of 25 mm diameter were provided as longitudinal flexural reinforcement and 5 bars with a diameter of 20 mm were included as longitudinal compression reinforcement. The diagonal bars and U-bars had a diameter of 16 mm, while the stirrups were 10 mm in diameter. The first 4 stirrups, closest to the nib, had two legs whereas deeper into the beam the shear reinforcement consisted of 3 legged stirrups.

Four different scenarios were tested, a reference specimen designed according to the principles discussed above, one specimen without the diagonal reinforcing bar but where the reinforcement layout was otherwise identical to that of the reference specimen, a specimen without the U-bars and finally a specimen with a reduced number of shear links. The three beams in which reinforcing bars were removed replicate rebar layouts that can be found in practice in structures from previous decades. They would no longer comply with current design codes and standards and hence no design load can be specified for these specimens. The different reinforcement layouts are shown in Fig. 4.

2.2. Materials

The reinforcement cages were constructed with ribbed reinforcing bars with a diameter of 10 mm, 12 mm, 20 mm or 25 mm. The nominal diameter ϕ, yield stress f_y (determined with the 0.2% offset method), and tensile strength f_u of the different steel reinforcing bars, were measured in the laboratory and are summarized in Table 2. The smaller reinforcing bars (10 mm or 12 mm) were cold deformed, whereas the larger bars were hot rolled.

The concrete was mixed on site in a volumetric truck. A common C30/37, according to European strength classes [38], was selected. The mix composition can be found in Table 3. A standard Portland cement CEM I complying with European Standard EN 197-1 [39] was used with a water-to-cement ratio of 0.53. The coarse and fine aggregates were a coarse 4/10 mm gravel and a sharp sand 0/4 mm, respectively. The grading curve for both materials can be found in Fig. 5. To achieve the desired workability class, a PCE superplasticiser was used. On casting, a slump of 75 mm was measured in accordance with EN 12350-2 [40].

All beams were cast at the same time and properly cured while hardening. After 72 h the beams were demoulded and stored in standard lab conditions of 21 ± 2 °C and a relative humidity of 70 ± 10%.

The strength development of the concrete was measured at an age of 1, 3, 7, 14, 28, 36 and 41 days by performing compressive tests on cubes with sides 100 mm ($f_{c,cub}$) and/or cylinders with diameter 100 mm and height 200 mm ($f_{c,cyl}$). At the time of testing, the beams had a strength between 50.8 MPa (NS-REF and NS-RS) and 52.0 MPa (NS-ND and NS-NU). In addition to the concrete compressive strength, the split tensile strength ($f_{ct,sp}$), the flexural tensile strength ($f_{ct,fl}$) and the modulus of elasticity (E_c) were measured. The results can be found in Table 4. The hardened density of the concrete was 2320 kg/m^3 and did not vary over time.

2.3. Test sequence and instrumentation

The specimens were tested in 3-point bending with the load applied in the centre of the specimen and the supports located underneath the nibs (Fig. 6). Based on the recommendations of Clark and Thorogood [12], roller steel bearings, with a steel roller with a diameter of 90 mm and 450 × 140 × 30 mm steel plates, were chosen as bearings. The force at each end was measured by a load cell and the deflection and deformation were recorded using linear variable displacement transducers. A total of 7 transducers were placed along the length of the beam and two transducers were positioned at each face of the beam to register the rotation of the free ends of the beam (Fig. 7).

The concrete strains were manually recorded on one side face of the beam after each load increment by means of mechanical strain gauges with an accuracy of 10^{-5}. The steel strains were recorded by means of strain gauges applied to the steel bars prior to casting. The strain gauge layout for the reference half-joint NS-REF is shown in Fig. 3. For each location one strain gauge was placed on the outermost reinforcing bar on one face and one on the outer-

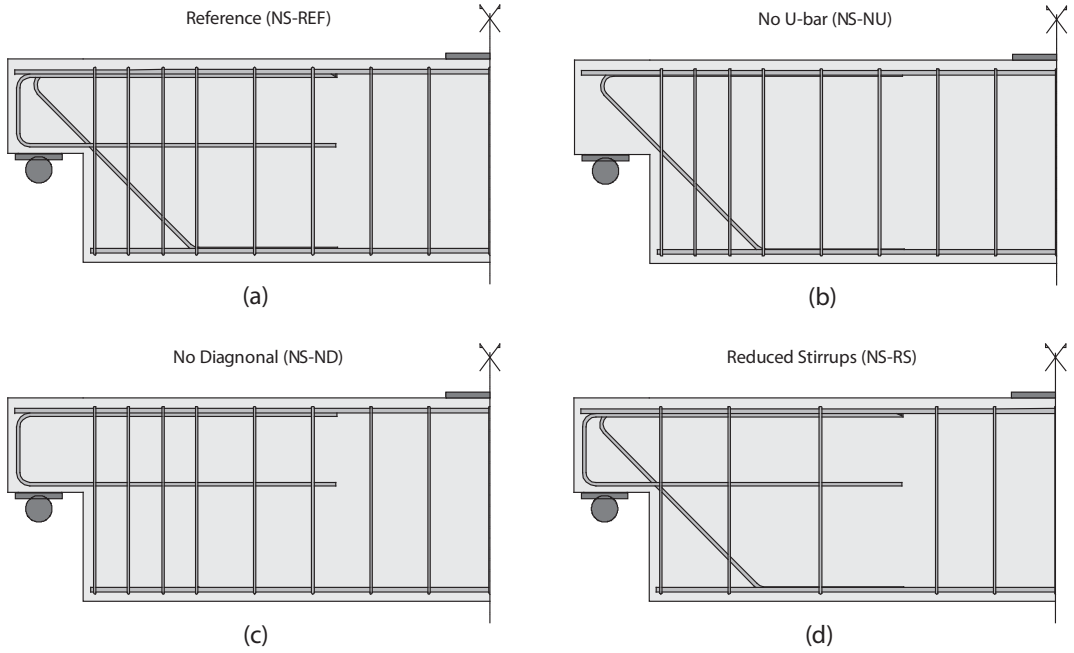

Fig. 4. Reinforcement layouts for the different test scenarios: (a) NS-REF, (b) NS-NU, (c) NS-ND, and (d) NS-RS.

Table 2
Mechanical and geometric characteristics of the reinforcing bars.

ϕ [mm]	f_y [MPa]	f_u [MPa]
10	539	596
12	529	559
25	578	674

Table 3
Concrete mix composition.

	Type	Amount [kg/m^3]
Cement	CEM I	320
Coarse aggregate	4/10 mm	1058
Fine aggregate	0/4 mm	829
Admixture	Superplasticiser	1.6
Water	–	170

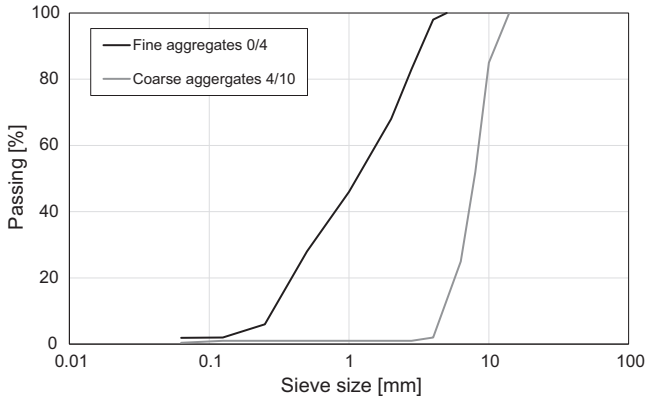

Fig. 5. Grading curves of fine and coarse aggregates.

most reinforcing bar on the other face (hence two measurements are available for each location). The same layout was used on the other beams with the exception that some of the bars were not present. On average 30 strain gauges per tested half-joint were installed.

During the first phase of testing, the force was increased stepwise until failure occurred at one end of the specimen. At this point, the specimen was unloaded. The support at the failed end was then moved inwards, supporting the full depth section of the beam (Fig. 6), and during the second loading phase, the load was again applied in a stepwise manner until failure of the second half-joint.

In contrast to studies where the beam is not supported on both nibs at the same time [16], the approach used in this study guarantees the half-joint ends are not loaded in unusual ways that differ from the actual loading situations.

3. Results

3.1. Overall behaviour

All specimens were loaded until failure. After each load increment, the crack pattern was marked on the beam surface (discussed later) and the concrete strains were manually measured from the mechanical strain gauge points. After the failure of the first end, the beams were thoroughly inspected and the support at the failed end was moved to the full-depth section. The recorded data showed that for all beams, the reinforcement stresses in the half-joint end that didn't fail in phase 1 were lower than the yield stress. No significant increase in the crack extension or number of cracks was noted during reloading when the applied load was lower than the maximum load reached during phase 1.

The highest failure load F_{max} of 402.3 kN was recorded for the reference specimen (Table 5). The failure occurred due to rupture of the diagonal and U-bar reinforcement at the location of the re-entrant corner (Fig. 8). The failure load was significantly higher than the original design load of 300 kN found using the strut-and-tie method. Similar differences have been reported previously by e.g. Ahmad and Elahi [35] who found that STM predictions ranged from a 50% underestimation to slight overestimations of the load capacity of reinforced concrete half-joints.

Table 4
Mean and standard deviation (between brackets) of concrete hardened properties at different concrete ages.

	Concrete age						
	1 days	3 days	7 days	14 days	28 days	36 days	41 days
$f_{c,cub}$ [MPa]	11.0 (0.8)	24.8 (1.2)	36.3 (1.6)	42.0 (1.4)	47.6 (2.3)	50.8 (1.0)	52.0 (1.7)
$f_{c,cyl}$ [MPa]	7.6 (0.5)	–	25.6 (1.2)	–	33.8 (1.0)	–	36.8 (3.2)
$f_{ct,sp}$ [MPa]	–	–	–	–	4.57 (0.15)	–	4.84 (0.11)
$f_{ct,fl}$ [MPa]	–	–	–	–	3.71 (0.18)	–	3.83 (0.25)
E_c [GPa]	–	–	–	–	33.7 (1.6)	–	34.6 (3.4)

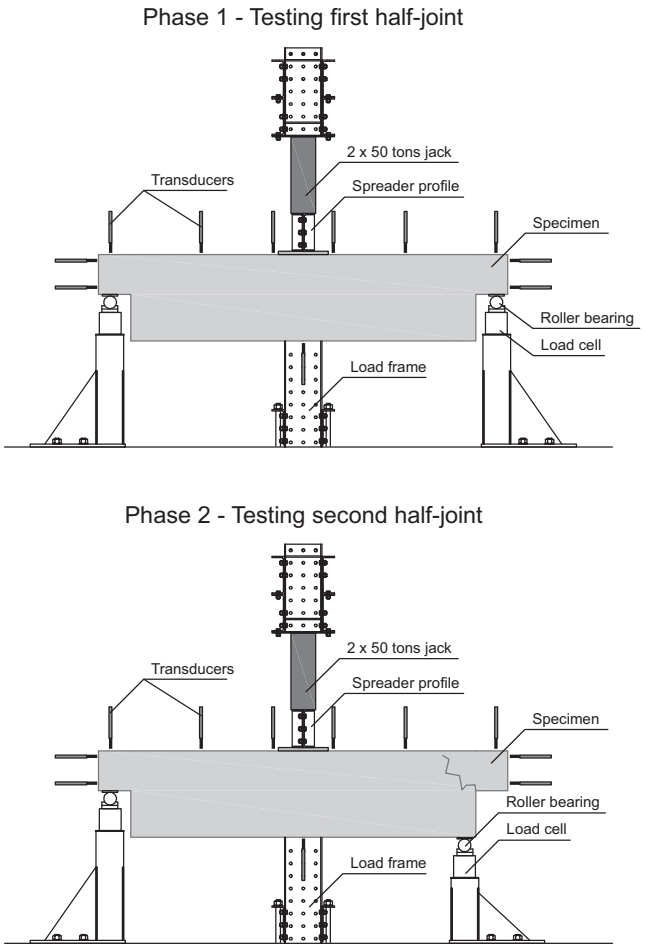

Fig. 6. Test set-up for 3-point bending experiments on reinforced concrete half-joint specimens.

By reducing the amount of shear reinforcement (NS-RS), the failure mode shifted from a nib failure to a full-depth shear failure. However, the reduction in overall capacity of the beam was only 8%, leading to a failure load of 358.0 kN. The absence of the U-bars had a bigger influence and resulted in the failure load dropping to 295.8 kN. The biggest reduction was measured when the 4 diagonal bars were removed. In that case, the load-bearing capacity of the specimen reduced to 244.9 kN, which is 39% lower than that of the reference specimen NS-REF.

The total mid-span deflection of the specimens when the maximum load was reached d_{peak} was in the range of 6.1–10.2 mm, as can be seen in Fig. 9. All specimens showed a similar load-deflection behaviour up to about 90–95% of their respective failure loads, at which point the deflection started to increase drastically due to the yielding of the reinforcement in the nib (specimen NS-REF, NS-NU, NS-ND) or yielding of the shear stirrups (specimen NS-RS).

Fig. 7. Test set-up for 3-point bending tests on half-joint beams.

3.2. Crack development and failure mode

As the re-entrant corner was not rounded or inclined [25], the first cracks in all the beams occurred at the re-entrant corner at a load between 99 and 107 kN (Table 5), corresponding to 27–42% of the ultimate load. The highest cracking load of 107 kN was recorded for the reference specimen due to the highest reinforcement ratio at the re-entrant corner. Similar observations were made by Barton [26] who reported first cracks at the re-entrant corner at load levels of 20–33% of the ultimate load.

Images of the final crack patterns are shown in Fig. 10, where the dominant cracks at the moment of failure are highlighted.

Shortly after the first cracks at the re-entrant corner developed, flexural cracks at the centre of the beam were detected. Both types of cracks gradually extended in length as the load increased. The length of the crack at the re-entrant corner for specimens NS-REF, NS-ND and NS-NU was comparable at similar load levels, indicating that the impact of the changes in the reinforcement layout on the crack length, for the given beam, were small. Whereas the number of flexural cracks (with small crack widths) increased, the number of cracks at the re-entrant corner was limited to one or two until the load reached values of about 200 kN.

For the NS-REF, NS-ND and NS-NU specimens, cracks parallel to the first re-entrant corner cracks started to develop when the load

Table 5
Failure loads, modes, and deformations for the reinforced concrete half-joints.

	F_{max} [kN]	F_{crack} [kN]	d_{peak} [mm]	Failure mode
NS-REF	402.3	107.0	10.2	Yielding of reinforcement bars at the nib
NS-ND	244.9	102.3	6.5	Yielding of reinforcement bars at the nib
NS-NU	295.8	100.5	6.1	Yielding of reinforcement bars at the nib
NS-RS	358.7	98.6	8.5	Shear failure in full-depth section

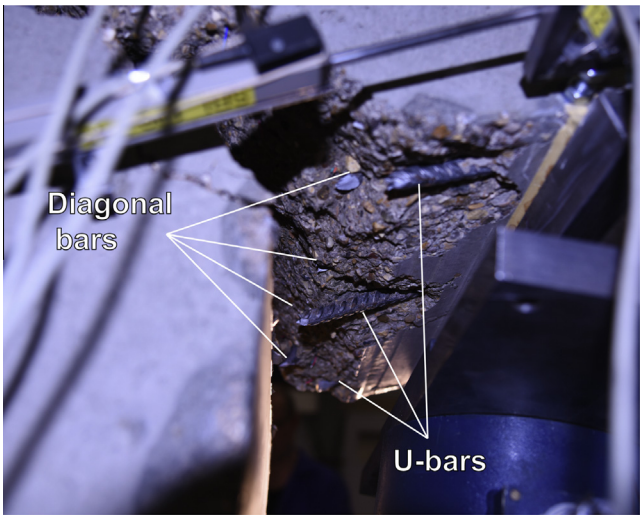

Fig. 8. Rupture of diagonal and U-bar reinforcement for the reference specimen NS-REF at failure.

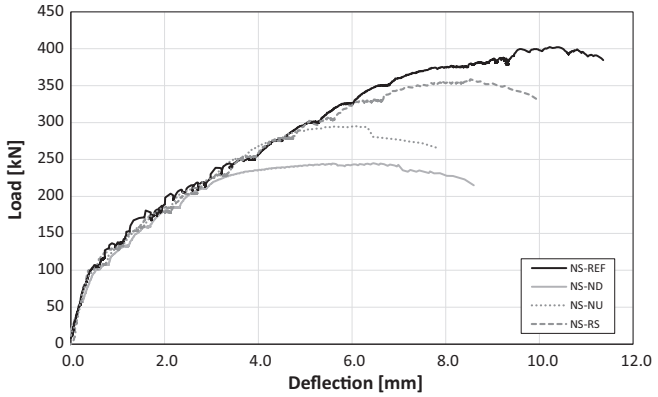

Fig. 9. Load - mid-span deflection curves for tested reinforced concrete half-joints.

exceeded 200–225 kN and the crack width also started to increase significantly (see discussion below). For specimens NS-NU and NS-RS significant cracking started to develop along the length of the first stirrup. The failure of NS-REF, NS-ND and NS-NU occurred by rupture of the reinforcing bars in the re-entrant corner leading to significant deformations and 'peeling-off' cracks occurring along the top reinforcement.

For the NS-RS specimen, the number of cracks in the re-entrant corner increased with increasing load. In addition, significant shear cracking in the full-depth section was observed. The spacing of the shear cracks was higher than for the reference specimen, as was to be expected due to the larger distance between the shear links. The failure occurred along a shear crack originating from the bottom corner of the full-depth section, one of the failure modes first mentioned by Hamoudi et al. [9] and Mattock and Chan [3] for half-joint beams which are under-reinforced in shear. This dominant crack only appeared at a load of 325 kN, but its crack width increased significantly as soon as a load of 350 kN was reached.

The angle of the first crack at the re-entrant corner for specimens NS-REF, NS-ND and NS-RS was around 40–45° relative the beam axis, which was consistent with the values of 40–60° reported by Wang et al. [15]. However, the first crack at this location for specimen NS-NU was significantly steeper, at an angle of 75°. As shown in Fig. 10, the dominant crack at failure for specimen NS-NU was, due to the absence of the U-bar, almost vertical.

The local deformations at the re-entrant corner were continuously measured using four transducers placed in a square arrangement (Fig. 11). As the base length of these transducers was only 100 mm, the measurements can be related to crack formation and crack opening at that location.

The deformations measured by the transducers TR-VERT-OUT and TR-HOR-TOP (placed on the nib side) were small for all specimens and showed in most cases a slight decrease with increasing load indicating compressive action in these regions. For TR-VERT-IN and TR-HOR-BOT (placed on the full-depth side), increasing lengths for increasing loads were measured. Fig. 12a shows the length increase measured by TR-VERT-IN for all specimens. As can be seen for load levels below 100 kN, little to no deformation is measured. As soon as the load exceeds the cracking load (discussed previously), an increase in deformation is measured. The biggest increase is noticed for NS-ND indicating larger initial crack widths than for the other specimens. The smallest deformations are measured for NS-REF due to the highest reinforcement concentration in the nib of all specimens tested.

For specimen NS-NU, the vertical deformation is smaller than measured for NS-RS and NS-ND. However, the horizontal deformation is significantly bigger. This confirms the earlier observation that the dominant crack in the nib for NS-NU was formed at an angle approaching vertical (hence being mostly picked up by the horizontal transducer) compared to angles of 45° for the other specimens.

Although specimen NS-RS (with reduced shear reinforcement) failed by means of a shear failure in the full-depth section of the beam, cracks are formed at the re-entrant corner and hence vertical as well as horizontal deformations are measured. The vertical deformations are largely in line with those for specimen NS-NU, while the horizontal are in line with NS-ND. Reducing the amount of shear reinforcement seems to have a smaller effect on the crack width and the extent of cracking than removing diagonal or U-bars. However, the measured deformations are still higher than those recorded for the reference beam.

3.3. Stress distribution

The steel strain gauge results can be analysed in terms of reinforcement steel stresses and total bar forces. The mean steel stress was calculated from the 2 strain gauge measurements recorded at the same location but on opposite faces of the beam. Fig. 13 shows the total bar forces (total force taken by all bars provided at that location) derived from the mean steel stresses at a load level of 240 kN. The level of 240 kN was selected as the highest level for which failure hadn't occurred in any of the specimens. As can be observed in Fig. 13, for the reference beam (NS-REF) the load of

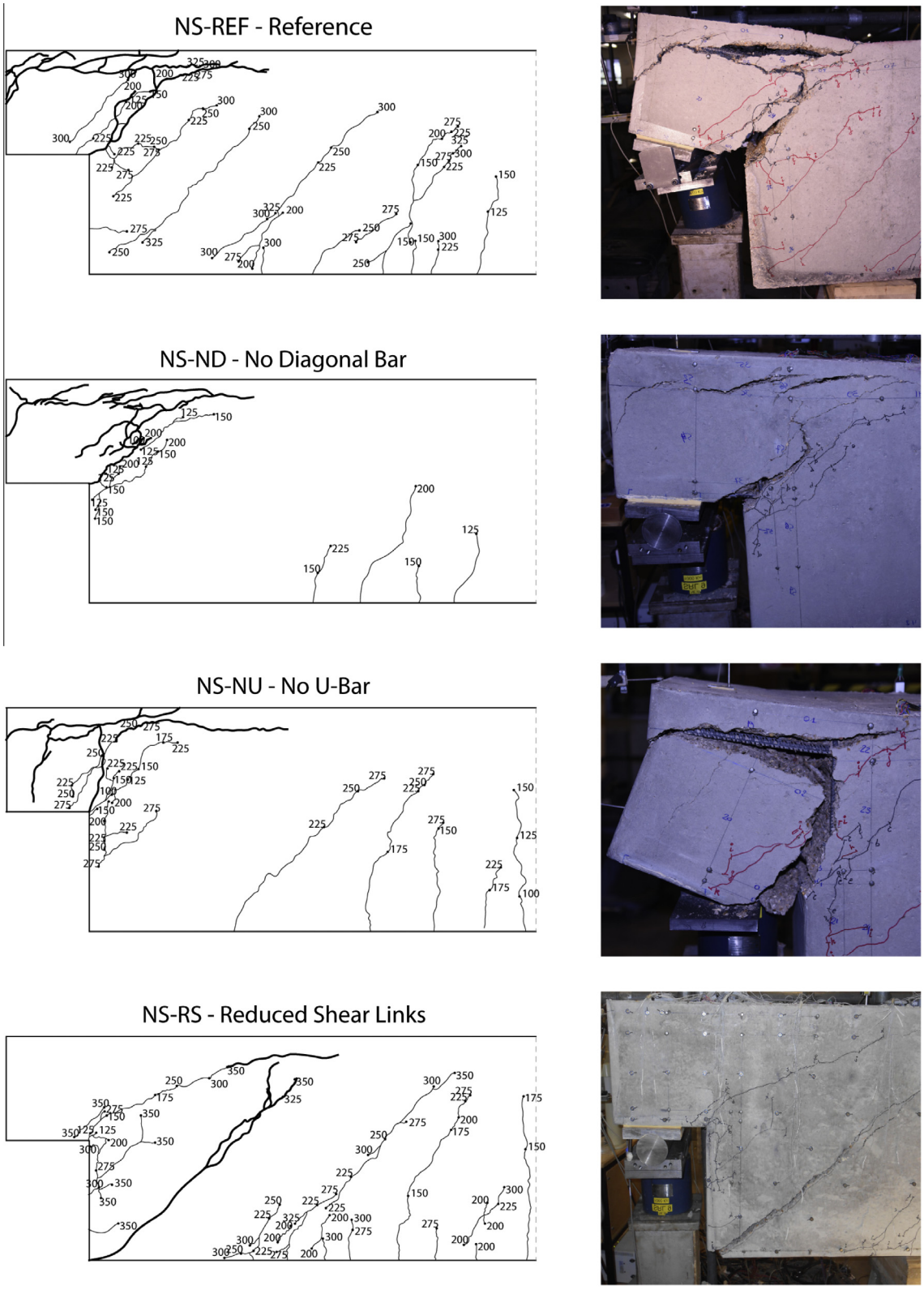

Fig. 10. Final crack pattern of tested reinforced concrete half-joint beams.

240 kN results in a total force of 89.9–92.0 kN being taken by the U-bars at the re-entrant corner, whereas the force in the diagonal bars is about 50% higher resulting in forces of 149.3 or 159.1 kN above and below the intersection. It is also of note that the cross-sectional area of the diagonal bars is 33% higher than the U-bars. For the applied load configuration tested in the current work, the forces taken by the stirrups are smaller with increasing distance away from the nib. Whereas the first stirrup sustains forces of 33.5–43.5 kN, the next stirrup takes 18.9 kN and the forces in the succeeding stirrups are smaller than 10 kN.

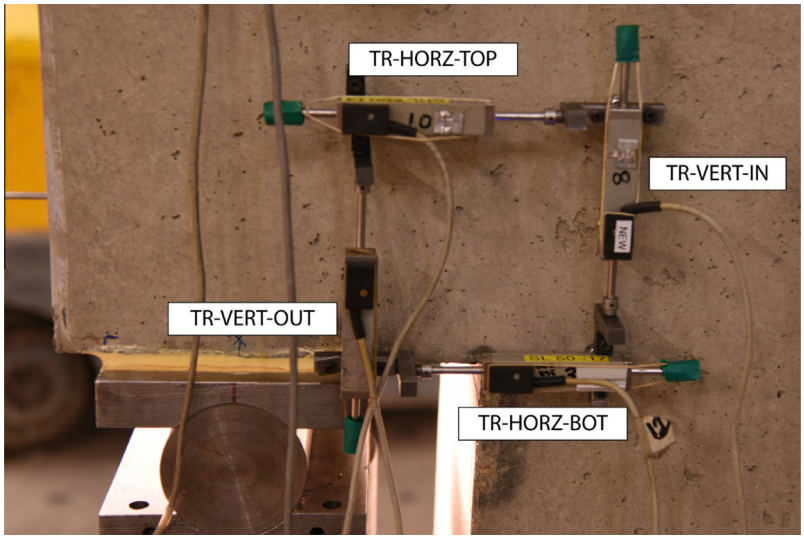

Fig. 11. Location of the transducers at the re-entrant corner.

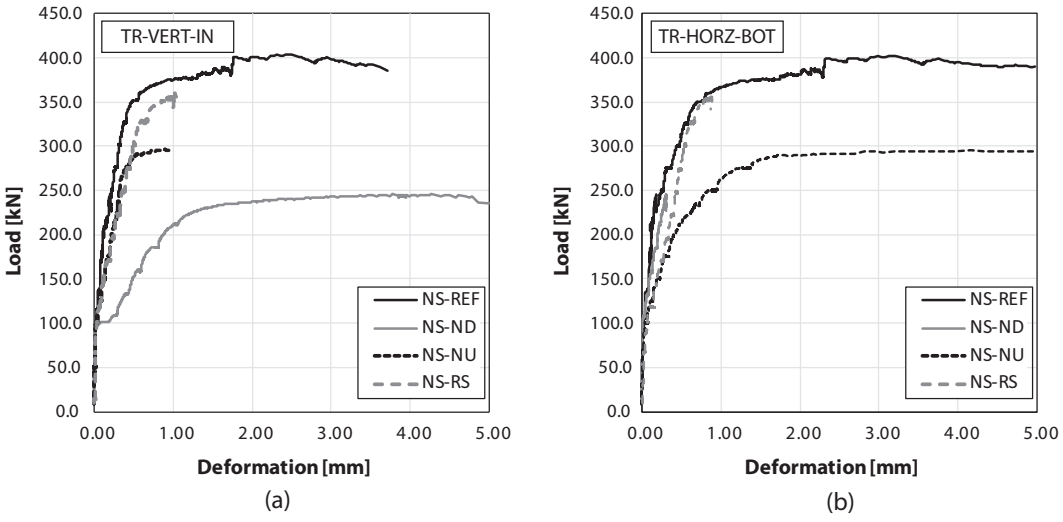

Fig. 12. Deformations measured at the re-entrant in (a) vertical direction by TR-VERT-IN and (b) horizontal direction by TR-HORZ-BOT.

When comparing the NS-REF reference specimen with the NS-NU specimen with no U-bars, there are significantly higher forces in the diagonal bars at a similar load level. The diagonal bar forces are 188.5–230.9 kN (relating to an increase of 16–35% with respect to the reference beam). The bar forces in the first stirrup are also higher, reaching values of 43.5–53.0 kN.

Even greater stirrup and U-bar forces are noted in the NS-ND specimen without diagonal reinforcement. The U-bar forces at a load level of 240 kN are approaching the maximum bar capacity (the 244.9 kN failure load of the specimen was close to this load level) and are yielding (the bar forces shown in Fig. 13 in bold, underlined and italic indicate yielding bars). The forces in the first stirrup are about 50% higher as well, clearly indicating a redistribution of forces and higher load demand on the remaining reinforcing bars.

The bar forces in the diagonal reinforcing bars for the NS-RS specimen with reduced shear reinforcement are comparable to those of the reference specimen. Reducing the shear reinforcement has little to no effect on the load carried by the diagonal bars. The U-bar forces are slightly higher, but the biggest increase relative to NS-REF is observed in the first stirrup (+45%).

The mean reinforcement steel stresses are presented in Fig. 14. All the reinforcing bars at the re-entrant corner of the reference specimen NS-REF were yielding (>529 MPa or 539 MPa) at failure. The U-bars and diagonal bars ruptured at failure as well as the first stirrup. Post-failure, the stresses in the second stirrup reached the yield stress as well. As several shear cracks developed in the specimen, the stresses in the stirrups in the full-depth section increased ranging from 231.1 to 311.9 MPa.

A similar observation can be made for specimens NS-NU and NS-ND. In both cases, the reinforcing bars at the re-entrant corner reached their yield stresses and finally ruptured. The stresses in the second stirrup reached yield values in NS-ND, while in specimen NS-NU the stresses in the second stirrup were much smaller (150.2 MPa). These lower stresses can be explained from the developed crack pattern. Whereas specimens NS-REF and NS-ND developed significant cracks at the re-entrant corner at an angle of about 45°, the dominant crack for specimen NS-NU was at an angle of about 80° (making it almost vertical). As a result, the second stirrup was not fully activated and was less efficient in increasing the load carrying capacity compared to the other two beams.

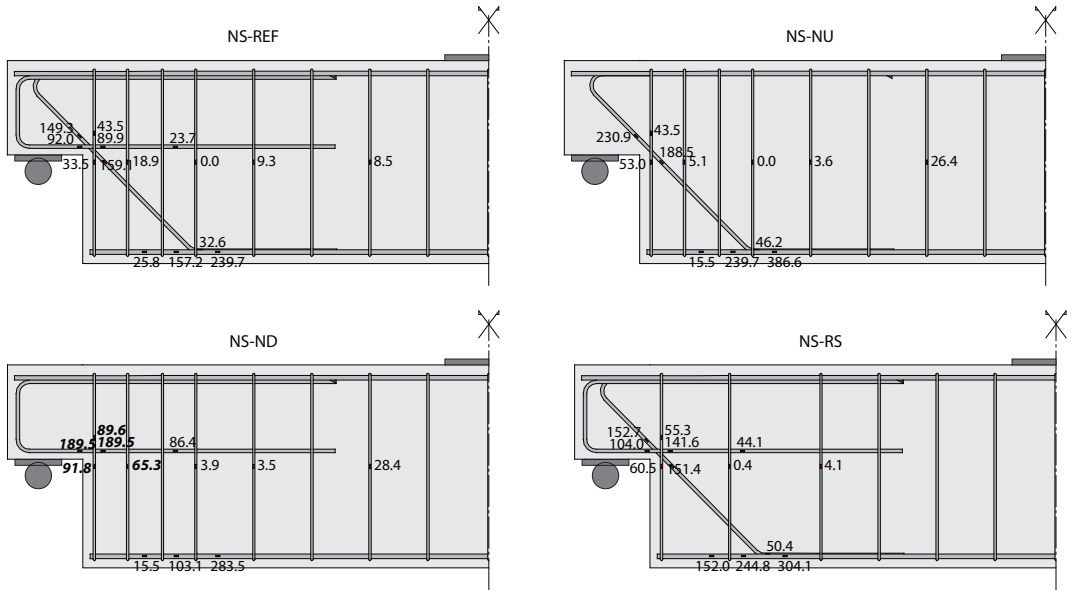

Fig. 13. Total bar forces of different specimens at a load of 240 kN.

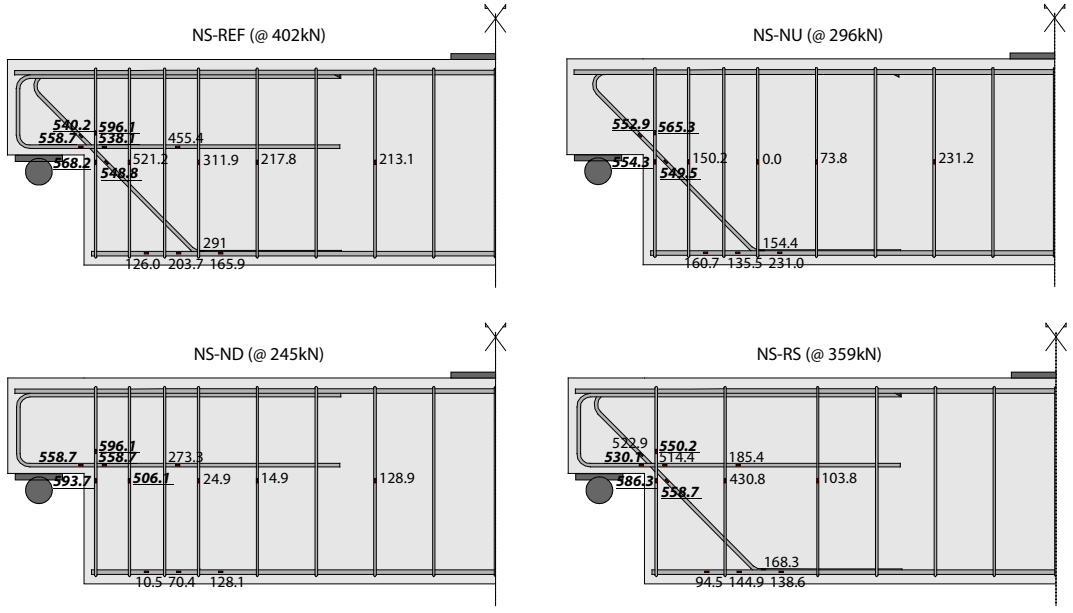

Fig. 14. Mean reinforcement bar steel stresses at failure load.

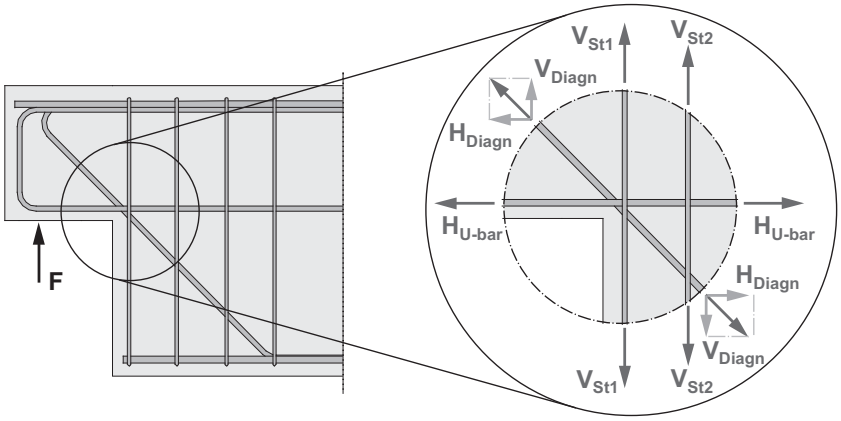

Fig. 15. Forces in the steel reinforcement at the re-entrant corner for specimen NS-REF.

Although specimen NS-RS failed in shear due to the limited shear reinforcement, the stresses in the reinforcing bars at the re-entrant corner were close to, or already exceeding the yield stress. This indicates that the specimen was close to a nib failure as well (which was to be expected since the failure load was approaching that of the reference specimen NS-REF). Since less shear reinforcement is provided, the stresses in the remaining stirrups are high with values of up to 430.8 MPa.

3.4. Force distribution in the nib

As noted in the previous section, the biggest impact on the bar forces was noted at the re-entrant corner. For the reference specimen NS-REF, the horizontal steel forces at the re-entrant corner are carried by the U-Bar, $H_{U\text{-}bar}$, and the horizontal component of the force in the diagonal bar H_{Diagn}. The vertical forces are taken by the vertical component of the force in the diagonal bar V_{Diagn} and

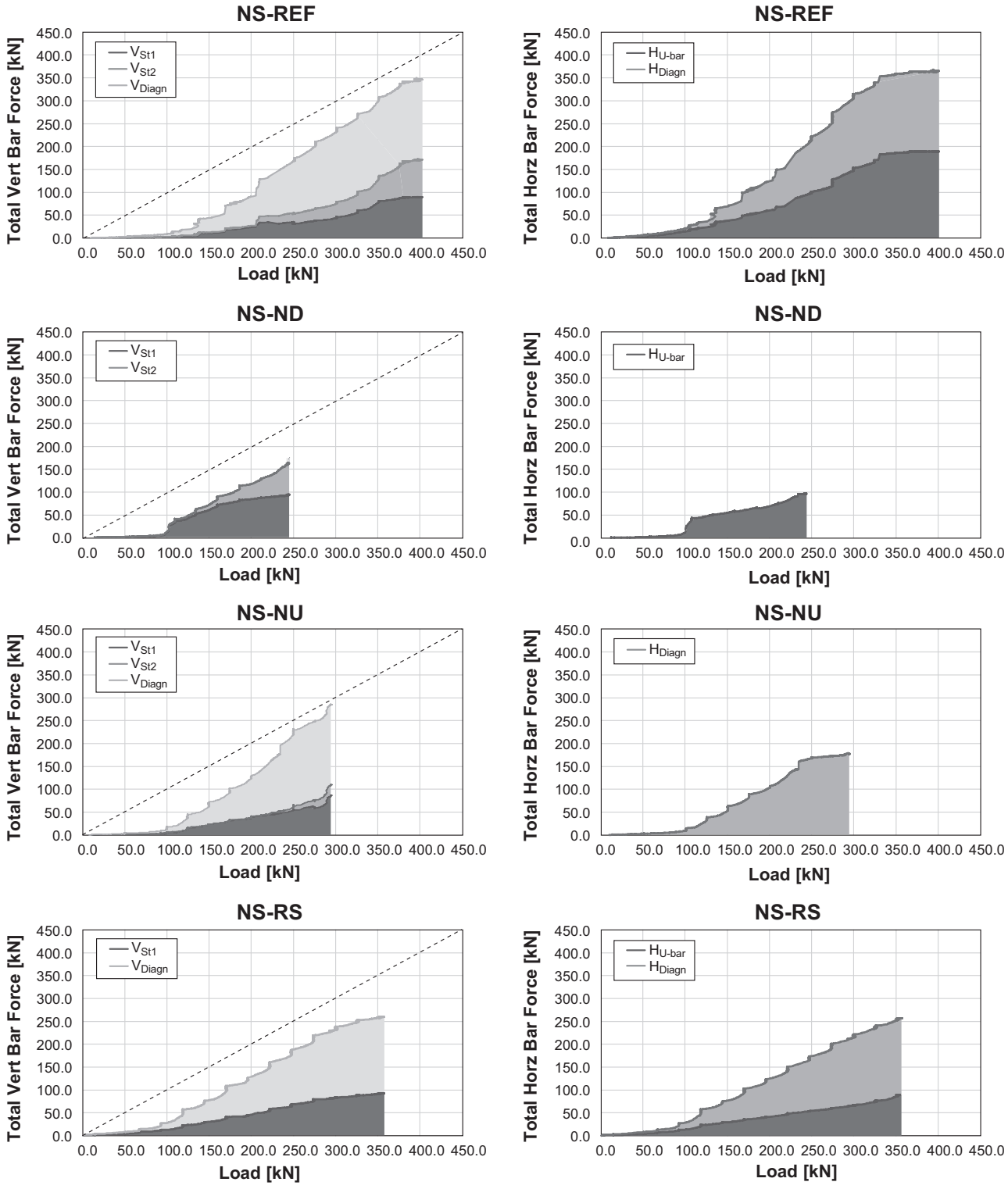

Fig. 16. Total horizontal and vertical bar forces at the inner nib for all tested specimens.

the contribution of the stirrups. Based on an STM design, the first two stirrups are assumed to contribute to the vertical tie at the nib, hence in the following discussion both vertical contributions V_{St1} and V_{St2} will be considered. The notation for the selected bar forces is shown in Fig. 15. As the load increases, and cracks are formed, the relative contribution of each forced component varies, e.g. in all specimens (except for NS-RS in which the second stirrup was absent) the second stirrup was activated when the crack initiated at the re-entrant corner had grown substantially. Hence it was only at higher loads that the vertical load was partly carried by stirrup 2 as well.

The evolution of the selected vertical and horizontal bar forces at the nib with increasing applied load is shown in Fig. 16. In the graphs of the vertical bar forces, the total applied vertical load F on the nib is indicated by a dashed line. For a free body that intersected only the selected bars, the difference between the dashed line and the vertical forces taken by the reinforcing steel bars are potentially taken by the concrete and dowel action of the U-bar and compression reinforcement.

For the reference specimen NS-REF, a total horizontal force of 368.3 kN builds up in the reinforcement by the time the failure load is reached. This force is divided into 51.5% carried by the U-bars (189.6 kN) and 48.5% carried by the diagonal bar (178.7 kN). The proportions for the total vertical reinforcement force of 350.6 kN are 51.0% for the diagonal bar, 25.5% for the first stirrup and 23.5% for the second stirrup. At lower load levels, the majority of the vertical reinforcement force is carried by the diagonal bar (up to 75% at 55 kN). The second stirrup didn't actively contribute to the overall force distribution until a load of 200 kN. At this point, the crack initiated at the re-entrant corner continued to grow and crossed the second stirrup. With respect to the horizontal reinforcement forces, the force is initially carried by the U-bar. However, at a load of 135 kN, the contribution from the diagonal bar increases from 35% to 45%.

Similar observations can be made for the other specimens. In the absence of a diagonal bar (specimen NS-ND), the horizontal reinforcement forces are carried solely by the U-bar. The total force in the U-bars at a load level of 245 kN is 96.5 kN. This number was comparable to the 94.1 kN force induced in the U-bars in the reference specimen at a similar load level. The vertical steel forces are fully carried by the stirrups. In comparison to the reference specimen, the second stirrup is activated much earlier and both bar forces are higher than the bar forces noted at a similar load level in the reference specimen. At the moment of failure, 54.0% of the reinforcement load (93.3 kN) is carried by the first stirrup, while 46.0% is carried by the second stirrup (79.5 kN).

When the U-bars are missing (specimen NS-NU), the horizontal force contribution from the reinforcement is solely due to the diagonal bars. The force taken by these bars at the moment of failure was 176.6 kN. The horizontal force taken by the diagonal bar in the reference specimen at the same load level was 156.0 kN. Hence the absence of the U-bars slightly increased the bar forces although to a lower level than the total horizontal bar forces in the reference specimen. The vertical reinforcement force in the NS-NU specimen was taken by both stirrups and the diagonal bar. Comparing the results with those of the reference specimen suggests similar trends in terms of the steel force distribution, although the contribution of stirrup 2 is significantly less. The reason for this might be found in the developed crack pattern. In the absence of a U-bar, the crack that initiated at the re-entrant corner showed a much steeper angle than the ~45° angle in the reference specimen (see Fig. 10). Hence the crack didn't cross the second stirrup until failure occurred. In addition, a steep increase in V_{St1} is noticed near failure. This increase is linked to the formation of a new crack at the re-entrant corner (running at an angle close to 90°) which evolved into the main failure plane (see Fig. 10).

The total horizontal bar force at failure measured for specimen NS-RS (with a reduced amount of shear reinforcement) of 256.9 kN was significantly lower than that for the reference specimen of 359.4 kN. The same conclusion applies to the total vertical reinforcement force. But it is of note that the failure mechanism of specimen NS-RS consisted of a shear failure in the full depth section of the beam instead of a nib failure.

4. Conclusions and further work

Previous research to determine the load carrying capacity of newly designed reinforced concrete half-joints has led to the current standards and guidelines. However, knowledge of the behaviour of half-joints with non-compliant reinforcement layouts is more limited and this can lead to problems when assessing existing structures. In this research program, four large-scale half-joint details with different reinforcement layouts were tested until failure. The performance of a reference specimen designed in accordance with current codes was compared with that of a beam where the diagonal reinforcing bars, the U-bars or some of the shear reinforcement was removed.

The following conclusions could be drawn from the test results:

- The reference specimen designed using a strut-and-tie model failed at a load which was higher than the design load indicating that current methods would provide a safe design for this particular reinforced concrete half-joint layout (assuming proper care is taken when detailing the reinforcement).
- In all specimens, cracks formed at the re-entrant corner at a load level corresponding to 20–33% of the failure load. The angle of this crack with respect to the longitudinal axis of the beams was around 40–45° for all specimens with the exception of the beam without a U-bar where the angle was significantly higher (75°).
- The deflections of the half-joint specimens were relatively small prior to failure.
- A brittle failure occurred at the re-entrant corner for the reference specimen, the specimen without diagonal reinforcement bars and the specimen without U-bars. In the case of the beam with a reduced amount of shear reinforcement, a shear failure occurred in the full-depth beam section.
- Reducing the amount of reinforcement in the half joint leads to a reduction in the load carrying capacity of the beams and influences the failure mode. Whereas removing the diagonal reinforcement or U-bar reinforcement in the nib leads to nib failure, the reduction of shear reinforcement led to a shear failure in the full-depth section of the beam. The greatest impact on the failure load was seen in the beam without diagonal reinforcing bars. The beam failed at 244.9 kN representing a load reduction of 39% compared with the reference specimen that failed at 402.3 kN. The impact of a reduced amount of shear reinforcement on the failure load was smaller and was around 10%.
- A redistribution of forces between the steel reinforcing bars was measured for the scenarios with insufficient reinforcement. The greatest amount of redistribution was observed in the reinforcing bars at the re-entrant corner.

The findings of this study show that the impact of improper reinforcement layouts might be significant. Clear reductions in the load carrying capacity are noted when reinforcing bars are omitted in the nib area. This has implications for strength assessments of existing structures with non-compliant reinforcement layouts. Additional experimental data is required in order to develop more accurate assessment techniques and to determine the potential for modifications to strut-and-tie models to account

for strength reductions associated with non-compliant details. This insight could also then lead to the formulation of revised recommendations for design.

Non-linear finite element models present a further analytical tool that could provide a predictive capability of half-joints with non-compliant internal reinforcement. However, as shown elsewhere [18], the obtained results and developed models require calibration and validation and are therefore typically only applicable to specific geometries and reinforcement layouts.

Acknowledgements

The authors would like to acknowledge the financial support of EPSRC – the Engineering and Physical Sciences Research Council (UK) – through the EPSRC Project 'Reinforced concrete half-joint structures: Structural integrity implications of reinforcement detailing and deterioration' [Grant no. EP/K016148/1].

Additional data related to this publication is available at the University of Cambridge's institutional data repository: http://dx.doi.org/10.17863/CAM.1735.

References

[1] Transport Scotland. TS Interim Amendment No. 20 - Concrete half-joint deck structures; 2006. p. 23.
[2] Loudon N. IAN 53/04 - Concrete half-joint deck structures; 2004. p. 18.
[3] Mattock A, Chan T. Design and behavior of dapped-end beams. PCI J 1979:28–45.
[4] Johnson P, Couture A, Nicolet R. Commission of inquiry into the collapse of a portion of the de la Concorde overpass – report; 2007.
[5] Mitchell D, Marchand J, Croteau P, Cook W. Concorde overpass collapse: structural aspects. J Perform Constr Facil 2011;25:545–53.
[6] fib Task Group 4.4. fib Bulletin 45 - Practitioners' guide to finite element modelling of reinforced concrete structures. Lausanne, Switzerland: International Federation for Structural Concrete (fib); 2008.
[7] Mitchell D, Cook W. Design of disturbed regions. Stuttgart; 1991.
[8] Prestressed Concrete Institute. PCI design handbook. 7th ed. Precast/Prestressed Concrete Institute; 2007.
[9] Hamoudi A, Phang M, Bierweiler R. Diagonal shear in prestressed concrete dapped-beams. ACI J 1975:347–50.
[10] Mitchell D, Cook W, Peng T. Importance of reinforcement detailing. ACI Spec Publ 2010;273:1–16.
[11] Steinle A, Rostasy F. Zum tragverhalten ausgeklinkter traederenden. Betonw + Fert 1975;41:270–7.
[12] Clark L, Thorogood P. Serviceability behaviour of reinforced concrete half joints. Struct Eng 1988;66:295–302.
[13] Moreno J, Meli R. Experimental study and numerical simulation of the behaviour of concrete dapped-end beams. Eng Model 2013;26:15–25.
[14] Moreno-Martínez J, Meli R. Experimental study on the structural behavior of concrete dapped-end beams. Eng Struct 2014;75:152–63.
[15] Wang Q, Guo Z, Hoogenboom P. Experimental investigation on the shear capacity of RC dapped end beams and design recommendations. Struct Eng Mech 2005;21:221–35. http://dx.doi.org/10.12989/sem.2005.21.2.221.
[16] Lu W-Y, Yu H-W, Lin I-J. Behaviour of reinforced concrete dapped-end beams. Mag Concr Res 2012;64:793–805.
[17] Lu W-Y, Chen T-C, Lin I-J. Shear strength of reinforced concrete dapped-end beams with shear span-to-depth ratios larger than unity. J Mar Sci Technol 2015;23:431–42.
[18] Boothman D, Leckie S, MacGregor I, Brodie A. Assessment of concrete half-joints using non-linear analysis. Proc ICE - Bridg Eng 2008;161:141–50.
[19] Taher S-D. Strengthening of critically designed girders with dapped ends. Struct Build 2005;158:141–52.
[20] Yang K-H, Ashour A, Lee J-K. Shear strength of reinforced concrete dapped-end beams using mechanism analysis. Mag Concr Res 2011;63:81–97.
[21] Watson J. Acoustic emission monitoring of concrete structures. In: Elsener B, editor. Proc first Work. COST 534 NDT Assess. New Syst. Prestress. Concr. Struct., Zurich, Switzerland; 2004. p. 31–44.
[22] Santhanam B, Shah P. Concrete half joint bridges in New South Wales: challenges in risk management. In: Austroads Bridg. Conf., Sydney. p. 497–511.
[23] Clark L. IAN53 half-joint assessment advice - ULS assessment of half-joints. Highways Agency; 2010.
[24] Lu W, Lin I-J, Hwang S-J, Lin Y-H. Shear strength of high-strength concrete dapped-end beams. J Chin Inst Eng 2003;26:671–80.
[25] Cook W, Mitchell D. Studies of disturbed regions near discontinuities in reinforced concrete members. ACI Struct J 1988;85:206–16.
[26] Barton D. Design of dapped beams using the strut-and-tie-model. University of Texas at Austin; 1988.
[27] Mader D. Detailing dapped ends of pretensioned concrete beams thesis. University of Texas at Austin; 1990.
[28] Bergmeister K, Breen J, Jirsa J, Kreger M. Detailing for structural concrete, Austin; 1993.
[29] ACI Committee 445–1. SP-208: examples for the design of structural concrete with strut-and-tie models. ACI International; 2002.
[30] Smith D. Refurbishment of the old Medway bridge, UK. Proc ICE-Bridge Eng, vol. 158. p. 129–39.
[31] Martin B, Sanders D. Verification and implementation of strut-and-tie model in LRFD bridge design specifications; 2007.
[32] Mohamed R, Elliott K. Shear strength of short recess precast dapped end beams made of steel fibre self-compacting concrete. In: Proc 33rd conf our world concr struct. Singapore: CI-Premier PTE Ltd.; 2008. p. 9.
[33] Amie N. Management of half joints in RTA bridges. In: Austroads Bridg. Conf. p. 1–12.
[34] Popescu C, Dăescu C, Tamás N, Sas G. Disturbed regions in dapped-end beams-numerical simulations of strengthening techniques. Nord Concr Res 2013;48:14–26.
[35] Ahmad S, Elahi A. Evaluation of the shear strength of dapped ended beam. Life Sci J 2013;10:1038–44.
[36] Aswin M, Mohammed B, Liew M, Syed Z. Shear failure of RC dapped-end beams. Adv Mater Sci Eng 2015;2015:11.
[37] ACI Committee 318. Building code requirements for structural concrete (ACI 318M-14) and commentary (ACI 318RM-14). 1st ed. Farmington Hills (MI), USA: American Concrete Institute; 2014.
[38] European Committee for Standardization. EN 1992-1-2 Eurocode 2: Design of concrete structures - Part 1–2: General rules - Structural fire design. European Committee for Standardization; 2008.
[39] European Committee for Standardization. EN 197-1:2011 - Cement - Part 1: Composition, specifications and conformity criteria for common cements. Brussels, Belgium; 2011.
[40] European Committee for Standardization. EN 12350–2:2009 - Testing fresh concrete: Slump-test. Brussels, Belgium: European Committee for Standardization; 2009.